© 2017. Published by The Company of Biologists Ltd | Development (2017) 144, 580-589 doi:10.1242/dev.147827

STEM CELLS AND REGENERATION

RESEARCH ARTICLE

A p53-based genetic tracing system to follow postnatal cardiomyocyte expansion in heart regeneration

Qi Xiao[1,2,*], Guoxin Zhang[1,*], Huijuan Wang[1], Lai Chen[1,3], Shuangshuang Lu[1,4], Dejing Pan[1,5], Geng Liu[1,‡] and Zhongzhou Yang[1,2,‡]

ABSTRACT

In the field of heart regeneration, the proliferative potential of cardiomyocytes in postnatal mice is under intense investigation. However, solely relying on immunostaining of proliferation markers, the long-term proliferation dynamics and potential of the cardiomyocytes cannot be readily addressed. Previously, we found that a *p53* promoter-driving reporter predominantly marked the proliferating lineages in mice. Here, we established a *p53*-based genetic tracing system to investigate postnatal cardiomyocyte proliferation and heart regeneration. By selectively tracing proliferative cardiomyocytes, a differential pattern of clonal expansion in *p53*$^{+}$ cardiac myocytes was revealed in neonatal, adolescent and adult stages. In addition, the percentage of *p53*$^{+}$ lineage cardiomyocytes increased continuously in the first month. Furthermore, these cells rapidly responded to heart injury and greatly contributed to the replenished myocardium. Therefore, this study reveals complex proliferating dynamics in postnatal cardiomyocytes and heart repair, and provides a novel genetic tracing strategy for studying postnatal cardiac turnover and regeneration.

KEY WORDS: Heart regeneration, Cardiomyocyte, Cell proliferation, *p53*, Lineage tracing, Mouse

INTRODUCTION

Pathological cardiac insults, such as myocardial infarction, cause irreversible cardiac remolding, myocardial fibrosis and impaired heart function, eventually leading to heart failure. For a long time, mammalian hearts have been considered to be non-regenerative due to the lack of detectable cardiomyocyte proliferation and absence of cardiac stem cells. However, this concept is being re-evaluated since Frisén and colleagues showed convincing evidence of human postnatal cardiomyocyte turnover using C^{14} enrichment quantification (Bergmann et al., 2009, 2015). Moreover, Lee's group reported that pre-existing cardiomyocytes underwent cell division to maintain cardiac turnover throughout the lifetime in mice (Senyo et al., 2013). The pioneering work performed by Sadek and Olson's groups in murine cardiac injury model showed that neonatal heart before postnatal day (P) 7 is able to regenerate completely after ventricular apex resection (Porrello et al., 2011). Genetic fate mapping demonstrated that replenished cardiac tissue is derived from pre-existing cardiomyocytes. Transplantation studies with non-cardiomyocytes cells, including cardiosphere-derived cells, bone marrow or stromal stem cells, also provided clues that endogenous cardiomyocyte proliferation could be activated by paracrine cytokines derived from grafted cells (Loffredo et al., 2011; Masuda et al., 2012). Taken together, these studies have demonstrated that both cardiac turnover and regeneration involve proliferation of pre-existing cardiomyocytes, indicating certain proliferative potential of postnatal cardiomyocytes (Laflamme and Murry, 2005).

Recently, the proliferative ability of cardiomyocytes in pre-adolescent mice has sparked heated debate (Alkass et al., 2015; Naqvi et al., 2014; Soonpaa et al., 2015). Naqvi and colleagues first reported a highly synchronized wave of cardiomyocyte proliferation between P14 and P15 during pre-adolescence, leading to a 40% increase of cardiomyocyte number (Naqvi et al., 2014). This study, however, was quickly challenged by two subsequent investigations. Using similar and alternative approaches with more precise and rigorous measurements, such as bromodeoxyuridine (BrdU)-containing osmotic mini-pumps, and Ki-67 (Mki67 – Mouse Genome Informatics) and phospho-histone H3 (PHH3) immunostaining to quantify DNA synthesis or through design-based stereology to determine the cardiomyocyte number in mouse hearts, these two studies reported very subtle cardiomyocyte expansion after P11-12 (Alkass et al., 2015; Soonpaa et al., 2015).

Most of these studies have been heavily dependent on immunostaining to detect cell proliferation [BrdU or ethynyl deoxyuridine (EdU) staining for DNA synthesis and Ki-67 or PHH3 staining for cell-cycle marker analysis]. These mostly transient assays do not allow measurement of the dynamic changes and lineage expansion of the proliferating cardiomyocytes over time, which is crucial for our understanding of their proliferative nature. Thus, a more convenient and robust methodology to investigate postnatal cardiomyocyte turnover in mice is urgently needed.

Early seminal findings have clearly established that *p53* (*Trp53* – Mouse Genome Informatics) mRNA expression and basal p53 expression were elevated by mitogen stimulation, fluctuated with cell cycle progression and were downregulated following differentiation (Dony et al., 1985; Reich and Levine, 1984). These were followed by many studies identifying key regulatory factors responsible for such expression pattern including Myc, E2F1 and C/EBP-β (Boggs and Reisman, 2007; Choi et al., 2002; Reisman et al., 1993). All these studies focused on the regulation of *p53* mRNA and p53 basal expression; however, this layer of regulation is distinct from the control of p53 protein stability, which is regulated by stress signaling through post-translational

[1]State Key Laboratory of Pharmaceutical Biotechnology and MOE Key Laboratory of Model Animal for Disease Study, Model Animal Research Center, Nanjing Biomedical Research Institute, Nanjing University, Nanjing 210061, China. [2]State Key Laboratory of Genetic Engineering, Collaborative Innovation Center of Genetics and Development, Fudan University, Shanghai 200438, China. [3]Jiangxi University of Traditional Chinese Medicine, 18 Yunwan Road, Nanchang, Jiangxi 330004, China. [4]Sino-British Molecular Cancer Center of Zhengzhou University, Zhengzhou, China. [5]Cambridge-Suda Genomic Research Center, Soochow University, 199 Renai Road, Suzhou 215123, China.
*These authors contributed equally to this work

‡Authors for correspondence (zhongzhouyang@nju.edu.cn; liug53@nju.edu.cn)

Z.Y., 0000-0002-3272-5255

Received 11 December 2016; Accepted 4 January 2017

Development (2017) 144, 580-589 doi:10.1242/dev.147827

modifications of both p53 and its negative regulator Mdm2, an E3 ubiquitin ligase (Haupt et al., 1997; Kubbutat et al., 1997). Thus, under normal conditions, p53 protein is continuously degraded and kept at very low levels, despite its highly elevated mRNA expression in proliferative compartments of tissues. Upon stress, p53 is rapidly stabilized by removal of the negative regulation by Mdm2 and is able to activate downstream targets in the proliferating cells where its basal level is high. Currently, there is no evidence supporting a link between regulation of p53 basal level expression and stress.

These studies established the foundation for us to use the *p53* promoter for cell proliferative analysis in mice and we observed that p53 expression closely reflects cellular proliferation as *p53* mRNA expression essentially parallels cell cycle progression (Chen et al., 2015). Although the precise function of *p53* transcription activity along with cell proliferation is not fully understood, it has been speculated that *p53* mRNA might provide a pre-translational pool ready for rapid and efficient response to cell stresses in cell cycle (Bourougaa et al., 2010). Accordingly, we generated a BAC transgenic mouse line containing a *p53* promoter-driving reporter that displayed preferentially high reporter activity in the proliferating compartments during tissue homeostasis and regeneration (Chen et al., 2015), indicating that the *p53* reporter could serve as a surrogate marker for cellular proliferation *in vivo*. Here, we introduced the Cre-ERT2 system under the control of *p53* promoter in a similar BAC transgenic setting. By crossing with *Rosa26*-ACTB-tdTomato-EGFP (*Rosa26*-mTmG), we established an inducible genetic tracing system to investigate the dynamics, clonal ability and tissue contribution of proliferating cardiomyocytes during mouse postnatal heart growth and regeneration.

RESULTS

Establishment of a *p53*-based genetic lineage-tracing system to study postnatal cardiomyocyte proliferation

We and others observed active cardiomyocyte proliferation in the first few days after birth (Fig. S1A-N) (Alkass et al., 2015; Senyo et al., 2013). We also examined the number of nuclei in the neonatal BrdU$^+$ cardiomyocytes. Consistent with a recent report (Alkass et al., 2015), we found only a very low percentage of BrdU$^+$ binucleated cardiomyocytes (Fig. S2A-D), indicating that multinucleation was minor at this stage. Therefore, detection of Ki-67, a well-established nuclear marker for cell proliferation, can reveal cardiomyocyte cycling during this stage.

Our previous study indicates that the *p53* reporter could serve as a surrogate marker for cell proliferation in murine tissues. Here, we applied this system to study cardiomyocyte proliferation in postnatal mice. For this purpose, we first compared the previously described *p53*-reporter expression (*p53*-BAC-nLacZ) with that of Ki-67 in the heart of neonatal mice. Immunofluorescence (IF) staining revealed colocalization of Ki-67 and β-galactosidase (β-gal) in the cardiomyocytes of P2 mice (Fig. 1A-C); 76.68±6.30% (s.e.m.) of Ki-67$^+$ cardiomyocytes were β-gal$^+$ and 70.01±1.14% of β-gal$^+$ cardiomyocytes expressed Ki-67, indicating that these two populations of cells were largely overlapping (Fig. 1D). To confirm cytokinesis of β-gal$^+$ cardiomyocytes, we co-stained for aurora B (aurora kinase B) and the cardiomyocyte marker cTnT (Tnnt2) in neonatal *p53*-BAC-nLacZ cardiac tissues. The results indicated that *p53*$^+$ cardiomyocytes were able to undergo cell division *in vivo* (Fig. 1E). Moreover, the *p53*$^+$ cardiomyocytes displayed cytomembrane localization of troponin proteins, which has been observed in cycling cardiomyocytes in both zebrafish and mouse models of heart regeneration (Fig. S3) (Jopling et al., 2010; Porrello et al., 2011).

In order to trace the proliferating cells genetically, we established BAC transgenic mice (*p53-Mer-Cre-Mer*) by inserting a *Mer-Cre-Mer-p53* 3′UTR cassette immediately after the first ATG of the BAC *p53* gene followed by pronuclear microinjection of the BAC construct (Fig. 1F). The *p53-Mer-Cre-Mer* mice were crossed with the *Rosa26*-mTmG mice to generate *p53-Mer-Cre-Mer*:*Rosa26*-mTmG (hereafter referred to as *p53*-mTmG) (no GFP expression was observed in these mice, data not shown). Injection of tamoxifen to these mice switched the expression of Tomato to GFP, thus permanently labeling the *p53* transcriptionally active (*p53*$^+$) cells and their progeny. GFP expression was examined in the cardiomyocytes 24 h after a single administration of tamoxifen to P1 *p53*-mTmG neonates (Fig. 1G). Quantification of GFP$^+$ cardiomyocytes revealed that ∼50% of these cells was also Ki-67$^+$ (GFP$^+$, Ki-67$^+$), representing a 5-fold enrichment of Ki-67$^+$ cells in the total cardiomyocyte population (Fig. 1H). In addition, the GFP$^+$ Ki-67$^-$ cardiomyocytes were frequently identified adjacent to GFP$^+$ Ki-67$^+$ cardiomyocytes in a two- to three-cell cluster, suggesting that they had recently exited the cell cycle (Fig. 1I). These results demonstrated that *p53*-mTmG genetic lineage-tracing system could detect and trace neonatal cycling cardiomyocytes.

In addition, we characterized and quantified the GFP$^+$ non-cardiomyocyte cells by cell-specific marker staining [CD31 (Pecam1) for endothelial cells and αSMA (Acta2) for vascular smooth muscle cells]. We found that a large number of endothelial cells were labeled by GFP, suggesting a robust continuous proliferating property (Fig. S4).

Clonal expansion of *p53*$^+$ cardiomyocytes in postnatal heart

To study the dynamics of cardiomyocyte proliferation in neonatal mice, a single pulse of a low dose of BrdU was administered to P1 mice and the heart sample was collected on P7 (Fig. S5A). BrdU staining displayed frequent nuclear BrdU$^+$ clusters consisting of five to eight cardiomyocytes, indicating a pattern of clonal expansion (Fig. S5B). To avoid dilution of labeling and the potential influence of the toxic effects of BrdU during long-term labeling, we aimed to trace the mitotic cardiomyocytes at single-cell resolution in *p53*-mTmG neonatal mice, by minimizing the dosage of a single injection of tamoxifen (10 ng/g body weight) (Fig. 2A). Single-cell labeling was confirmed by administration of tamoxifen to P3 or P7 mice and analyzing the hearts 1 day later (Fig. 2A-C). For cardiac myocyte clonal formation analysis, hearts were dissected 2 weeks after tamoxifen administration (Fig. 2A). GFP$^+$ cardiomyocyte clusters were clearly identified when the labeling was initiated in the neonatal mice (Fig. 2D,E). Interestingly, clusters of GFP$^+$ cardiomyocytes were also observed in the hearts of pre-adolescent and adult mice using a similar strategy (Fig. 2F-L). We quantified the size and number of these clusters in hearts from neonatal, pre-adolescent and adult stages. The ability of cardiomyocytes to multiply dropped only slightly between P3 and P7, then gradually decreased further at the pre-adolescent and adult stages (Fig. 2M,N). Intriguingly, a few of the labeled cardiomyocytes seemed to be not only able to preserve their proliferating ability until adult stage, they also formed larger clusters if given longer tracing time (Fig. 2M,N), suggesting their selectively long-lasting proliferative potential.

To confirm that the GFP$^+$ cardiomyocyte clusters are derived from single cells, we crossed the *p53-Mer-Cre-Mer* and *Confetti* mice to generate another tracing model (*p53-Confetti*) based on the Brainbow 2.1 system. The Confetti (Brainbow 2.1) system is

Development (2017) 144, 580-589 doi:10.1242/dev.147827

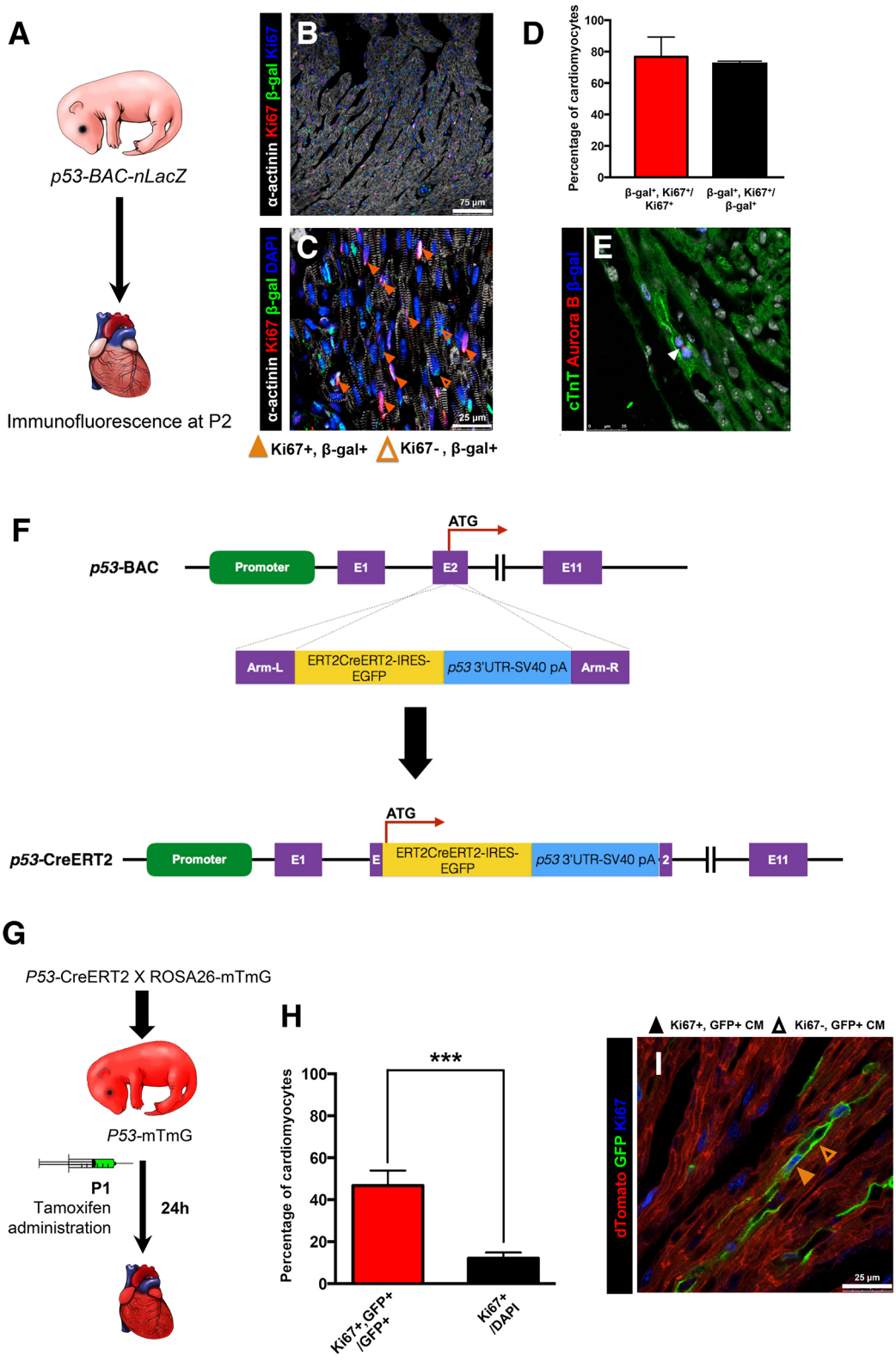

Fig. 1. Establishment of a *p53*-based genetic lineage-tracing system to study postnatal cardiomyocyte proliferation. (A) Diagram to show that heart was harvested from *p53*-BAC-nLacZ mice at P2 for immunofluorescence (IF) staining. (B) IF staining for α-actinin, Ki-67 and β-gal (*p53* reporter). Scale bar: 75 µm. (C) Higher magnification of B. Scale bar: 25 µm. Filled arrowheads indicate Ki-67$^+$ β-gal$^+$; open arrowheads indicate Ki-67$^-$, β-gal$^+$. (D) Quantification of distinct population of cardiomyocytes. *n*=5 for each group. (E) IF staining for aurora B (indicated by arrowhead). (F) Construct for generating inducible *p53-Mer-Cre-Mer* mice. (G) Diagram showing the procedure of generating the *p53*-based genetic lineage-tracing system (*p53*-mTmG) and tamoxifen administration. Tamoxifen was injected into P1 mice and the heart was harvested 24 h later for IF staining. (H) Quantification of Ki-67$^+$ cardiomyocytes in GFP$^+$ cardiomyocytes as well as in total cardiomyocytes. *n*=5 for each group. (I) IF staining of adjacent GFP$^+$ cardiomyocytes. Note that the GFP$^+$ Ki-67$^+$ cardiomyocytes (filled arrowheads) were frequently identified adjacent to GFP$^+$ Ki-67$^-$ cardiomyocytes (open arrowheads) in a two- to three-cell cluster. Scale bar: 25 µm.

Development (2017) 144, 580-589 doi:10.1242/dev.147827

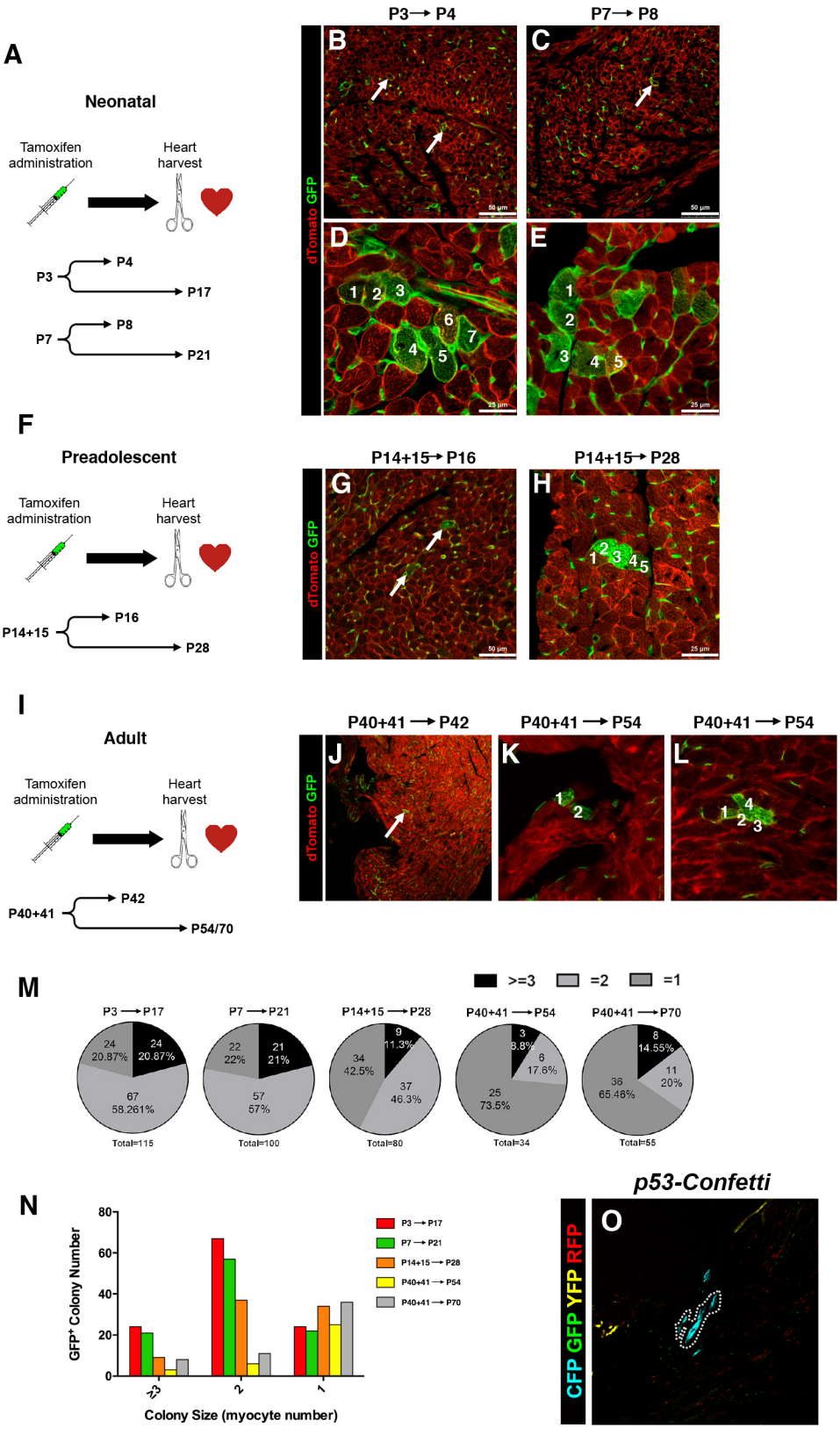

Fig. 2. Clonal expansion of *p53*$^+$ cardiomyocytes in postnatal heart. (A-E) Genetic tracing of *p53*$^+$ lineage cardiomyocytes in neonatal mice. (A) Diagram showing time points for tamoxifen administration and heart collection. Tamoxifen dosage is 10 ng/g body weight. (B,C) IF imaging revealed initial GFP labeling of cardiomyocytes (indicated by arrows) at single-cell resolution, marked by arrows. (D,E) IF imaging showing clonal expansion of *p53*$^+$ lineage cardiomyocytes 2 weeks after tamoxifen administration. A 7-cell clone (D) and a 5-cell clone (E) are shown. (F-H) Lineage tracing of *p53*$^+$ lineage cardiomyocytes in pre-adolescent heart. (F) Diagram showing time points for tamoxifen administration and heart collection. (G) IF imaging revealed initial GFP labeling of cardiomyocytes (indicated by arrows) at single-cell resolution. (H) IF imaging showing clonal expansion of *p53*$^+$ lineage cardiomyocytes. (I-L) Lineage tracing of *p53*$^+$ lineage cardiomyocytes in adult heart. (I) Diagram showing time points for tamoxifen administration and heart collection. (J) IF imaging revealed initial GFP labeling of cardiomyocytes (indicated by arrow) at single-cell resolution. (K,L) IF imaging showing clonal expansion of *p53*$^+$ lineage cardiomyocyte. A 2-cell clone (K) and a 4-cell clone (L) are shown. (M,N) Quantification of *p53*$^+$ lineage cardiomyocyte clones of distinct size from the neonatal, pre-adolescent and adult tracing analysis. (O) Clonal analysis of heart tissue in *p53-Confetti* mice. Dotted line encircles a clone. Scale bars: 50 µm (B,C,G), 25 µm (D,E,H).

currently recognized as one of the optimal tools for clonal analysis in mice. Two weeks after a single tamoxifen injection to *p53-Confetti* mice at P3, we observed clonal cardiomyocyte patterns (Fig. 2O; Fig. S6). These results further demonstrated the clonal expansion of *p53*$^+$ cardiomyocytes in postnatal mouse heart.

It was reported that cardiomyocytes under hypoxic conditions (Hif1α$^+$ population) at the neonatal stage display proliferative potential and form clones *in vivo* (Kimura et al., 2015). These two lineages (*p53*$^+$ and Hif1α$^+$) display similar characteristics of proliferative potential and clonal expansion. Therefore, we

Development (2017) 144, 580-589 doi:10.1242/dev.147827

investigated whether they were the same population. To test the Hif1α antibody, we first treated HEK293 cells with $CoCl_2$ (positive control) and PBS (negative control) and collected these cells for Hif1α staining. The results were convincing and we then examined the Hif1α-positive cardiomyocytes in *p53*-mTmG neonatal cardiac tissues. We failed to detect double-positive cardiomyocytes (Hif1α$^+$ and GFP$^+$) (Fig. S7), suggesting that *p53*$^+$ and Hif1α$^+$ are two distinct populations in postnatal mouse heart.

In summary, by permanently labeling the once-proliferating cardiomyocytes, the new genetic tracing system has clearly demonstrated a lasting, albeit decreased cloning expansion property of the postnatal *p53*$^+$ cardiomyocyte lineage from neonatal to adult stages.

Activation of the *p53*$^+$ cardiomyocyte pool by injury in neonatal mice

The clonal expansion property of *p53*$^+$ lineage cardiomyocytes is suggestive of a strong proliferative ability, which could be evaluated by the accumulation and contribution of the *p53*$^+$ cardiomyocyte lineage in mouse heart. For this purpose, two high doses of tamoxifen were consecutively administered to the *p53*-mTmG mice at P1 and P2 and the GFP$^+$ cells were traced up to one month of age. We found a continuous increase of GFP$^+$ cardiomyocyte contribution to the heart, amounting to at least 10% at one month of age (Fig. 3A, control group). This result does indeed indicate a more potent cell proliferation of *p53*$^+$ lineage cardiomyocytes.

Injury activates cardiomyocyte proliferation to repair damaged myocardium in neonatal mice (Porrello et al., 2011). We, therefore, studied the cell behavior of *p53*$^+$ lineage cardiomyocytes in an injury model. Non-penetrating cryo-injury (CI) was induced in the left ventricle of neonatal mice that were capable to completely repair injured myocardium. A comprehensive anatomical and histological analysis confirmed successful construction of the injury model (Fig. S8A-K). Two pulses of high dose (200 µg/g body weight) tamoxifen were administrated to *p53*-mTmG mice at P1 and P2, followed by cryo-injury at P5 (Fig. 3A). In the sham group, *p53*$^+$ lineage cardiomyocytes displayed a similar pattern of accumulation as the control group (Fig. 3A). In contrast, injury enormously activated *p53*$^+$ lineage cardiomyocytes, and 1 week after the injury the percentage of these cells reached 12.5% in undamaged myocardium compared with 8% in the sham group (Fig. 3A), and eventually to nearly 25% by one month (Fig. 3A). Quantitative analysis of the cells in the injured area revealed that up to 70% of them were GFP$^+$ (Fig. 3B). Due to indiscernible sarcomeric pattern, it was hard to quantify accurately the number of GFP$^+$ cardiomyocytes in the damaged area (Fig. S8K). By morphological study, we considered that approximately 30% of the cardiomyocytes were GFP$^+$.

Together, these results demonstrated that the *p53*$^+$ neonatal cardiomyocytes represented potent proliferative ability and were activated by injury in neonatal mice.

p53$^+$ cardiomyocytes exhibit cytomembrane localization of cTnT in heart regeneration

Previously, it was reported that cycling cardiomyocytes displayed cytomembrane localization of sarcomeric proteins, such as cTnT, in regenerating murine and fish hearts (Jopling et al., 2010; Porrello et al., 2011). We observed this phenomenon in *p53*$^+$ cardiomyocytes at the neonatal stage and wondered whether *p53*$^+$ cardiomyocytes showed a similar pattern of troponin proteins in cryo-injured heart. Indeed, we observed many cardiomyocytes with cytomembrane localization of cTnT in whole ventricular sections from cryo-injured heart but not from the sham group at P35 (Fig. 4A-H). This suggested that these GFP$^+$ cardiomyocytes were activated to enter proliferative status. Cytoskeletal disorganization of cardiomyocytes is considered essential for re-entering the cell cycle. cTnT interacts with actin and tropomyosin, which is involved in myosin contraction in muscular cells. To test whether cytomembrane localization of cTnT in p53$^+$ cardiomyocytes results from disorganization of the cytoskeleton, we co-stained cTnT and α-actinin in neonatal cardiomyocytes. The results revealed cytomembrane localization of cTnT in cardiomyocytes with intact α-actinin forming sarcomere, suggesting that cytomembrane localization of cTnT is independent from cytoskeletal disorganization (Fig. 4I-K).

Primary contribution of *p53*$^+$ lineage cardiomyocyte to heart regeneration in neonatal mice

In our cryo-injury model, the majority of fibrotic scars were replenished with functional cardiomyocytes within one month (Fig. S9A-C). *De novo* coronary arteriogenesis, a sign of regeneration, was observed in the repaired myocardium (Fig. S9B,C). Histological study revealed many more GFP$^+$ cardiomyocytes in the repaired myocardium compared with the myocardium in the sham group (Fig. 5A-D). A more detailed quantitative analysis of different areas in the myocardium of repaired heart [*de novo* left ventricle (*dn*LV), ventricular septum (VS) and right ventricle (RV)] indicated that 35.53±1.63% cardiomyocytes in the *dn*LV were GFP$^+$ (Fig. 5E), compared with that of other regions (20% for RV and 15% for VS) (Fig. 5E). In addition, a large number of GFP$^+$ cardiomyocytes in the *dn*LV displayed a clonal pattern (Fig. 5F,G).

To verify further the contribution of the *p53*$^+$ cardiomyocyte lineage in heart regeneration, we traced this lineage in another two types of cardiac damage models: apex resection and left coronary artery ligation (LCAL) (Fig. 6A-G). Neonatal mice were

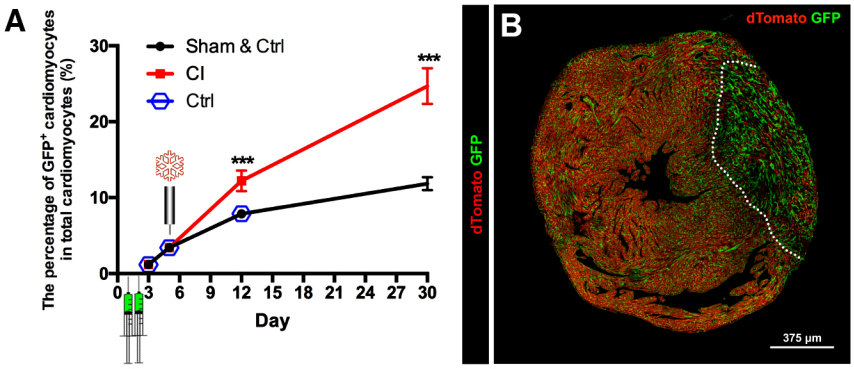

Fig. 3. Activation of *p53*$^+$ cardiomyocyte pool by injury in neonatal mice. (A) Dynamic change of *p53*$^+$ lineage cardiomyocytes. Note the continuous increase of GFP$^+$ cardiomyocyte percentage in normal mice (Ctrl). Cryo-injury (CI) caused an enormous increase of GFP$^+$ cardiomyocyte percentage compared with the sham group. Data represent mean±s.d. from at least five independent experiments. (B) IF tile-scanning of ventricular section showing the *p53*$^+$ lineage cells (GFP$^+$) 1 week after the cryo-injury induction. Dotted line marks the injured area. Scale bar: 375 µm.

Development (2017) 144, 580-589 doi:10.1242/dev.147827

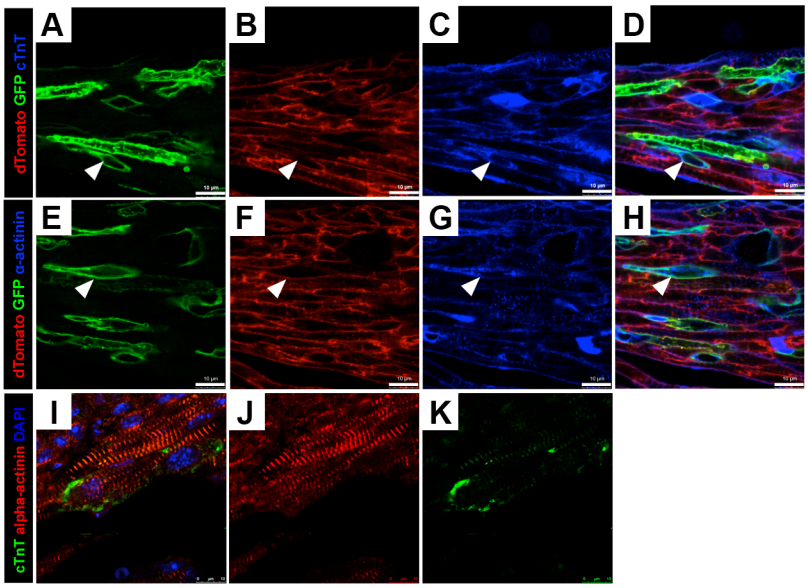

Fig. 4. Imaging of p53$^+$ cardiomyocytes in cryo-injured heart. (A-H) IF staining showing cytomembrane localization of cTnT (indicated by arrowheads in A-D) and of α-actinin (indicated by arrowheads in E-H) of GFP$^+$ lineage cardiomyocytes. Scale bars: 10 µm. (I-K) Cytomembrane-localized cTNT in cardiomyocytes with intact sarcomeric structure.

administered with a single pulse of tamoxifen at a dosage of 100 µg/g body weight at P1 and surgeries (apex resection and LCAL) were performed at P5 using a simple and convenient method as previously described (Fig. 6H) (Mahmoud et al., 2014). Histological analysis confirmed the success of these surgeries (Fig. 6B-G). To evaluate the contribution of the *p53*$^+$ cardiomyocyte lineage in cardiac repair, we harvested the hearts and quantified the percentage of GFP$^+$ cardiomyocytes in the ventricles. Similar to the results for the cryo-injury model, we observed significantly increased GFP$^+$ cardiomyocytes in both groups of damaged hearts (Fig. 6I,J).

Collectively, these results demonstrated that *p53*$^+$ lineage cardiomyocytes primarily contributed to heart regeneration.

DISCUSSION

Previous studies, based on Levine and others' observations (Harris et al., 2005; Vousden and Lane, 2007), indicated a preferential expression of *p53* mRNA in the proliferating cellular compartment of various tissues in mice (Chen et al., 2015). In this study, we reported the establishment of a novel *p53*-based lineage-tracing system that faithfully recorded and traced cardiomyocyte proliferation in postnatal mice. Compared with the popular transient labeling techniques for cell proliferation analysis, such as Ki-67 and PHH3 staining, our *p53*-reporter lineage-tracing system demonstrated better sensitivity and accuracy. For instance, either Ki-67 or PHH3 staining cannot distinguish cardiomyocyte multinucleation and polyploidization in pre-adolescent heart. Besides, it is rather hard to label cycling cardiomyocytes in adult heart with these two techniques due to extremely low cycling rate. Although BrdU labeling can distinguish cardiomyocyte mitosis from multinucleation and nuclear polyploidization, it cannot follow cellular behavior of specific lineages over a long term. By contrast, our *p53*-reporter lineage-tracing system has the advantage of being able to permanently label the ever-proliferative cardiomyocytes and follow their fate, expansion

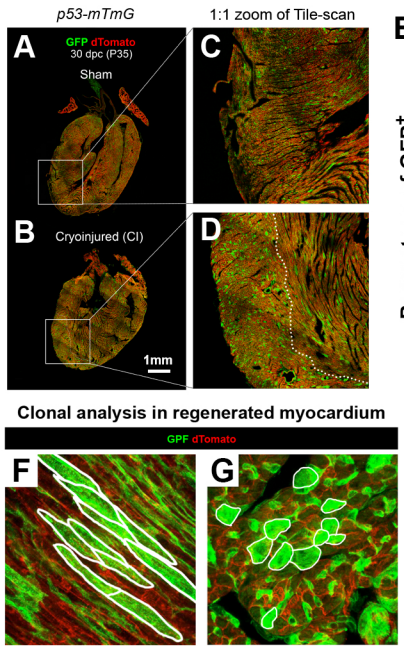

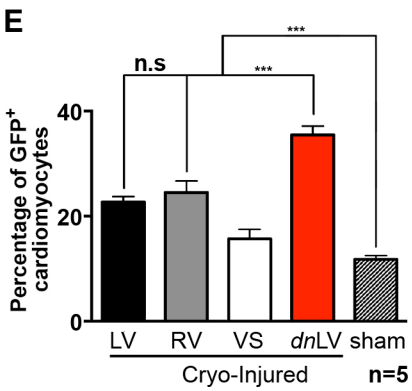

Fig. 5. Primary contribution of *p53*$^+$ lineage cardiomyocytes to heart regeneration (cryo-injury model) in neonatal mice. (A-D) IF imaging showing *p53*$^+$ lineage cardiomyocytes in the sham and repaired myocardium. The dotted line marks the boundary of *de novo*-formed myocardium. (E) *p53*$^+$ lineage cardiomyocytes occupancy in different parts of myocardium. LV, left ventricle; RV, right ventricle; VS, ventricular septum; *dn*LV, newly formed (*de novo*) left ventricular myocardium. (F,G) IF imaging showing GFP$^+$ cardiomyocyte clusters (white lines) in different regions.

Development (2017) 144, 580-589 doi:10.1242/dev.147827

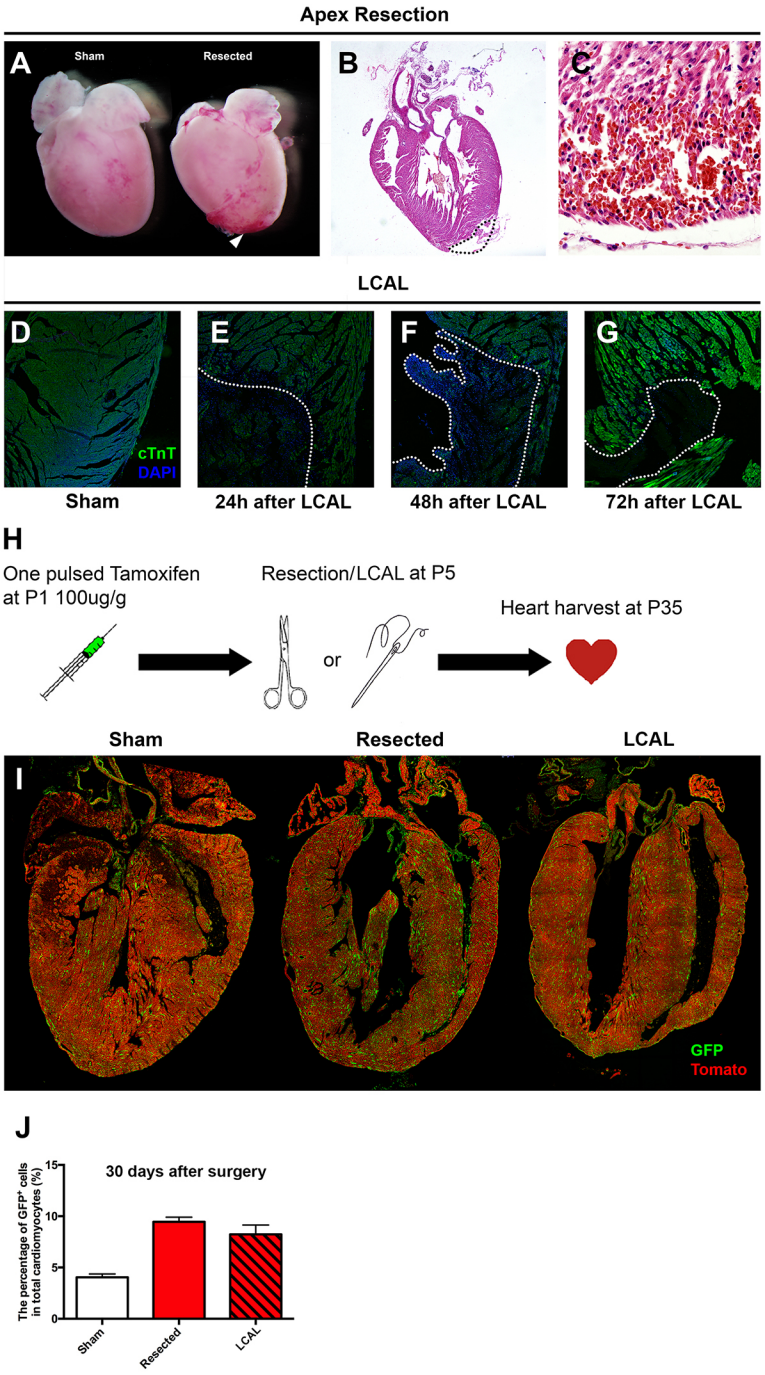

Fig. 6. Primary contribution of *p53*$^{+}$ lineage cardiomyocytes to heart regeneration (apex resection and LCAL model) in neonatal mice. (A-C) Evaluation of apex resection surgery. Hearts were dissected 1 day after surgery. (A) Gross analysis. Arrowhead indicates the resected area. (B,C) Histological analysis. (B) Resected area is marked with a dotted line. (C) Hemorrhage in the border area after apex resection. (D-G) Evaluation of LCAL surgery. Lack of cTNT staining indicates the infarcted area (marked by dotted line). (H) Schematic of heart regeneration in apex resection and LCAL models. (I) Tile scanning of sections of regenerated hearts. (J) Quantification of GFP^{+} cardiomyocytes.

property and contribution in the whole tissue, thus allowing a thorough evaluation of the proliferating dynamics.

Hence, our *p53*-based lineage-tracing system can complement the existing methodologies to better follow up and document the cellular behavior and events of postnatal mitotic cardiomyocytes, even at single-cell resolution. Using this system, we demonstrated a lasting clonal expansion property of postnatal cardiomyocytes and documented the robust response of *p53*$^{+}$ lineage cardiomyocytes to injury.

This study revealed that the contribution of GFP^{+} cardiomyocytes was continuously increased after birth. Furthermore, some *p53*$^{+}$ cardiomyocytes were able to maintain the clone-forming activity well into the adult stage. These results uncovered a frequent re-entry into cell cycle of the *p53*$^{+}$ lineage, suggesting more potent proliferative ability of this lineage and proliferative heterogeneity of cardiomyocytes in mice. This kind of proliferative heterogeneity of cardiomyocytes was discovered in newts and zebrafish (Bettencourt-Dias et al., 2003; Kikuchi et al., 2010). Our results implicate that this phenomenon is conserved in mammalian heart.

Consistent with the attenuated clonal expansion properties of cardiomyocytes at P14-15, genetic tracing also revealed only a moderate increase of GFP^{+} cells in the myocardium of the heart between P12 and P30, thus not supporting a proliferation burst at the pre-adolescent stage in mice (Naqvi et al., 2014).

This study also demonstrated a robust response of the *p53*$^{+}$ cardiomyocyte lineage to injury. By one month after injury, the representation of *p53*$^{+}$ lineage cardiomyocytes reached nearly one-quarter in the myocardium. The representation was even higher

Development (2017) 144, 580-589 doi:10.1242/dev.147827

(~40%) in the *de novo*-formed myocardium. Thus, $p53^+$ cells are a major source for heart regeneration in these cardiac injury models. The proliferative heterogeneity of cardiomyocytes was clearly observed in the process of heart repair, pinpointing the significance of the phenomenon.

The limitation of the *p53* genetic tracing system is that its labeling of proliferative cells is not cell specific. In cardiac tissue, it marks all proliferating cells including cardiomyocytes, endothelial cells, fibroblasts and vascular smooth muscle cells. However, it is practically feasible to discern these cell types through a combination analysis of cell-specific markers and morphology. On the other hand, our approach cannot define the cellular origin of the new cardiomyocytes contributing to heart repair.

In summary, the present study has demonstrated the identification of a specific cardiomyocyte lineage contributing to neonatal murine heart growth and regeneration. It also provides a novel genetic tracing strategy for studying postnatal cardiac turnover and repair.

MATERIALS AND METHODS

Generation of *p53-Mer-Cre-Mer* BAC transgenic mouse

The experimental animal facility has been accredited by the Association for Assessment and Accreditation of Laboratory Animal Care International (AAALAC), and the Institutional Animal Care and Use Committee (IACUC) of the Model Animal Research Center of Nanjing University approved all animal protocols used in this study.

An ERT2CreERT2-IRES-EGFP cassette followed by *p53* 3′UTR-SV40 poly A cassette was inserted into *p53* BAC (No.bMQ-441J16) at the ATG codon in the second exon of *p53* gene via recombination. The loxp and loxp511 sites in the BAC backbone were replaced by *Amp* and *Kan* expression cassette. The final BAC was purified by Nucleo Bond^R max100 BAC extraction kit (MACHERERY-NAGEL), and was then verified by sequencing and restriction enzyme mapping. To generate the BAC transgenic founders, 1.0 ng/µl of the purified BAC in microinjection buffer was injected. These founders were first screened by long-fragment PCR to ensure the integrity of the BAC copy in these mice. The desired founders were then bred with *Rosa26*-LacZ reporter mice to have the germline transmission. The expression pattern of the Cre recombinase in these BAC transgenic mice was verified by X-gal staining upon tamoxifen injection. Primer sequences for genotyping were as follows: Cre: 5′-GCGGTCTGGCAGTAAAAACTATC-3′ and 5′-GTGAAACAGCATTGCTGTCACTT-3′; Rosa-mT/mG: 5′CTCTGCTGCCTCCTGGCTTCT-3′, 5′CGAGGCGGATCACAAGCAATA-3′ and 5′-TCAATGGGCGGGGGTCGTT-3′.

Heart mass analysis

Hearts were dissected and were immersed into Ca^{2+}/Mg^{2+}-free PBS for 10 min. Cleaned hearts were fixed with 4% paraformaldehyde for 2 h and then cut in two halves along the ventricular septum. The two parts were immersed into a 2 ml Eppendorf tube with 1 ml PBS. For semi-quantitative analysis of heart mass, distilled water was carefully added into another 2 ml centrifugal tube with 1 ml water until the fluid levels in both tubes were indistinguishable. The volume of added water is equivalent to the mass of myocardium. Three hearts were measured for each group.

Histology

Heart samples were fixed in 4% paraformaldehyde overnight at room temperature. Afterwards, the heart samples were dehydrated through immersion into 35%, 50%, 75%, 85% and 95% ethanol each for 30 min. Then the heart samples were transferred into 100% ethanol for 1 h twice. After dehydration, heart samples were immersed in xylene at room temperature for 5-20 min, depending on sample mass, and were then transferred into fresh paraffin at 65°C for 60 min three times before paraffin embedding. Sections were processed for Hematoxylin and Eosin staining. Masson's trichrome staining was performed as previously reported (Di et al., 2012).

Immunofluorescence (IF) staining

IF staining was performed on paraffin, frozen or fresh sections. For the paraffin sections, antigen retrieval was performed for 30 min in sodium citrate buffer. Slides were rinsed three times in TBS with 0.05% Triton X-100 (TBST) and blocked in 10% goat serum for 1 h at room temperature followed by three 5 min rinses in TBST. Sections were incubated overnight at 4°C with primary antibodies against troponin T (1:200, mouse monoclonal, NeoMarker, MS-295-P0), α-actinin (1:200, rabbit polyclonal, clone H-300, Santa Cruz, sc-15335), Ki-67 (1:200, mouse monoclonal, clone MIB-1, DakoCytomation, M724901), β-gal (1:50, Abcam, ab9361), Aurora B (1:500, Abcam, ab2254), Hif1 alpha (1:50, Novus, NB100-105) and BrdU (1:200, rat monoclonal, BU1/75, AbD Serotec, MCA2060). The following day, sections were washed in TBST four times (5 min each wash) and incubated with anti-mouse, -rat, -rabbit, -goat and -chicken secondary antibodies conjugated to Alexa Fluor 488 or Cy3 (all from Jackson Immunoresearch, 1:500, goat anti-mouse Alexa Fluor 488, 115-545-166; goat anti-mouse Cy3, 115-165-166; goat anti-rabbit Cy3, 111-165-144; goat anti-rabbit Alexa Fluor 488, 111-545-144; goat anti-rat Alexa Fluor 488, 112-545-167; goat anti-rat Cy3, 112-165-167; donkey anti-goat Cy5, 705-175-147; goat anti-chicken Cy3, 103-005-155) for 2 h at room temperature. After incubation, slides were rinsed three times (10 min each) in TBST and mounted in 50% triglyceride.

For wheat germ agglutinin (WGA) staining, slides were deparaffinized, rinsed three times in PBS and then incubated for 1 h at room temperature with primary antibody against WGA conjugated to Alexa Fluor 594 (50 µg/ml, Invitrogen) in PBS. Slides were then rinsed three times in PBS, stained with DAPI and mounted in 50% triglyceride.

For the frozen sections, samples were usually fixed in 4°C for 2 h. The cardiac tissues for β-gal staining were fixed on ice for 4 h to prevent β-gal degeneration. Fixed tissues were transferred to 30% sucrose with 0.1% sodium azide (NaN_3) for sedimentation. Once samples were on the bottom of centrifugal tubes, they were transferred into frozen section medium (Thermo Scientific Pink Neg-50 No. 6502P) and the medium was quickly frozen in liquid nitrogen for several seconds. All frozen embedded samples were stored at −80°C and 10-µm-thick sections were prepared for IF staining or imaging with confocal laser microscopy just before use. Frozen tissues were rinsed in TBST for 1 min five times and blocked with 10% goat serum for 1 h in room temperature. Afterwards, samples were incubated in primary antibody solution against β-gal, cTnT and α-actinin at 4°C overnight. The secondary antibody system was the same as for the paraffin wax-embedded sections.

For the fresh sections, samples were embedded in 12% low melting point agarose gel and sliced (50 µm) using vibratome for IF staining. Antibody treatment is similar to frozen sections. *Z*-stack imaging (over 30µm) is performed to study the binucleated cardiomyocytes in neonatal mouse heart.

BrdU incorporation

Bromodeoxyuridine (BrdU, Sigma) was administered to mice by intraperitoneal injection (1 mg per 10 g body weight). Heart samples were dissected and fixed in 4% paraformaldehyde, then further processed for IF staining as described above.

Computer-assisted analysis of binucleated cardiomyocytes

Fresh ventricular tissues were sectioned (50 µm) with a vibratome on both transverse and coronal planes. Sections were stained with WGA and DAPI for labeling cell membrane and nuclei, respectively. In each section, only the cardiomyocytes with myofibril orientation parallel to the longitudinal plane were counted. The region of interest (ROI) was marked crossing ten cardiomyocytes in each section and signal curves of both WGA and DAPI were recorded automatically following *z*-stack scanning. The dynamic signal curves and image animations were analyzed for binucleation identification. The data from ten sections of one heart at multiple anatomical positions were defined as a group of values of a single sample. Each group consisted of five samples for statistical analysis.

Genetic cell lineage tracing

p53-Mer-Cre-Mer BAC transgenic mice were crossed with *Rosa26*-ACTB-tdTomato-EGFP (*Rosa26*-mTmG, from the Jackson Laboratory, Stock No.

Development (2017) 144, 580-589 doi:10.1242/dev.147827

023035) mice to generate a tamoxifen-inducible *p53* genetic lineage-tracing system (*p53*-mTmG mice). Tamoxifen dissolved in sesame oil (Sigma) was injected into stomachs of neonatal mice (from newborns to P5). For mice older than P5, tamoxifen was administrated intraperitoneally. For lineage mapping during cardiac regeneration, tamoxifen was administered to neonates from P1 to P3 with a dosage of 200 µg/g/day for maximal labeling of proliferating cardiomyocytes. The hearts were harvested for IF imaging. For single-cell tracing, the working concentration of one/two-pulses of tamoxifen was diluted to 20 µg/g for minimal labeling. Heart samples were harvested for IF imaging.

Imaging and tile-scan imaging

IF images were captured with a Leica SP5 confocal laser microscope. For photon quantification, images were recorded with HyD detector in SP5. To measure protein enrichment in single cells or subcellular fractions, ROI was applied for zone selection and matrix pattern of quantification was exported with protogenous Leica software. For high-resolution images of the transverse plane of the ventricle, tile-scan imaging was performed by joining hundreds of fields of view (FOV) of a 40× field lens. Each tile-scan image can be amplified to cellular resolution.

Cryo-injury (CI) surgery

Cryo-injury surgery was performed in neonates. The mice were first anesthetized by cooling on ice. The skin was sterilized with 75% ethanol, followed by lateral thoracotomy at the fourth intercostal space to expose the left ventricle, as previously reported (Porrello et al., 2011). A pre-cold sterile stainless steel tool in liquid nitrogen was taken out for 10 s and then touched the surface of the exposed left ventricle chamber for 5 s. Following CI, the intercostal muscles rebounded and the chest was closed. Cut skin was conglutinated with medical adhesive. After surgery, all neonates were isolated from maternal mice for half a day. The entire surgery procedure was usually accomplished within 5 min and 95% neonates survived. In the following 24 h, the operated neonates showed less movement than the sham-operated mice. However, they were indistinguishable from the sham mice at later stages of regeneration. Carprofen (4.5 µg/kg) was administered to surviving mice for analgesia.

Apex resection and left coronary artery (LCA) ligation

In this new method of myocardial infarction induction, mice were anesthetized with 2% isoflurane with an isoflurane inhalation delivery system (Viking Medical, Medford, NJ, USA) but not ventilated. Before perfecting this surgical model, we recommend using ventilation in mice until the surgeon can routinely perform the LCA ligation in 3 min. A small skin cut (1.2 cm) was made over the left chest, and a purse suture was made as shown in Fig. 1A-C. After dissection and retraction of the pectoral major and minor muscle, the fourth intercostal space was exposed. A small hole was made at the fourth intercostal space with a mosquito clamp to open the pleural membrane and pericardium. With the clamp slightly open, the heart was smoothly and gently 'popped out' through the hole. The LCA was located, sutured and ligated at a site 3 mm from its origin using a 6-0 silk suture. The ligation was deemed successful when the anterior wall of the LV turned pale. After ligation, the heart was immediately placed back into the intrathoracic space followed by manual evacuation of air and closure of muscle and the skin, by means of the previously placed purse-string suture. The mouse was then allowed to breathe room air and monitored during the recovery period, which was generally complete within 3-5 min. No artificial respiratory aid was required during the recovery time. The sham group underwent the same surgical procedure except that the LCA was not occluded.

Statistical analysis

Results are presented as mean±s.e.m. Statistical analyses were performed using GraphPad Prism 6.0. For comparisons between two groups, statistical significance was determined using an unpaired two-tailed Student's *t*-test. For comparisons of multiple groups, one-way ANOVA followed by Tukey's multiple-comparison test was carried out. A value of $P<0.05$ (*) was considered statistically significant and $P<0.01$ (**) as well as $P<0.005$ (***) was considered statistically very significant.

Acknowledgements

The authors thank Drs Xingxu Huang and Ying Xu for their valuable help with this work.

Competing interests

The authors declare no competing or financial interests.

Author contributions

Q.X. and G.Z. designed and conducted the experiments, Q.X. and G.Z. performed the majority of the experiments and analyzed data from all experiments with D.P., G.L. and Z.Y. IF staining, BrdU labeling and *p53* genetic lineage tracing were performed by Q.X., G.Z. and H.W. Q.X., H.W. and S.L. performed the surgery. L.C., G.Z. and G. L. generated *p53-nLacZ* and *p53-Mer-Cre-Mer* mice. Q.X., G.L. and Z.Y. prepared and edited the manuscript.

Funding

This work was supported by grants from the National Natural Science Foundation of China (31130037, 31571490, 91519312, 31071282, 91149000 and 91019002 to Z.Y.; 30871265 and 31171305 to G.L.), and grants from the National Key Basic Research Program of China (Ministry of Science and Technology of the People's Republic of China) (2012CB966600 and 2011CB943904 to Z.Y.) and the State Key Laboratory of Genetic Engineering of Fudan University (SKLGE-1604 to Z.Y.).

Supplementary information

Supplementary information available online at
http://dev.biologists.org/lookup/doi/10.1242/dev.147827.supplemental

References

Alkass, K., Panula, J., Westman, M., Wu, T.-D., Guerquin-Kern, J.-L. and Bergmann, O. (2015). No evidence for cardiomyocyte number expansion in preadolescent mice. *Cell* **163**, 1026-1036.

Bergmann, O., Bhardwaj, R. D., Bernard, S., Zdunek, S., Barnabe-Heider, F., Walsh, S., Zupicich, J., Alkass, K., Buchholz, B. A., Druid, H. et al. (2009). Evidence for cardiomyocyte renewal in humans. *Science* **324**, 98-102.

Bergmann, O., Zdunek, S., Felker, A., Salehpour, M., Alkass, K., Bernard, S., Sjostrom, S. L., Szewczykowska, M., Jackowska, T., dos Remedios, C. et al. (2015). Dynamics of cell generation and turnover in the human heart. *Cell* **161**, 1566-1575.

Bettencourt-Dias, M., Mittnacht, S. and Brockes, J. P. (2003). Heterogeneous proliferative potential in regenerative adult newt cardiomyocytes. *J. Cell Sci.* **116**, 4001-4009.

Boggs, K. and Reisman, D. (2007). C/EBPbeta participates in regulating transcription of the p53 gene in response to mitogen stimulation. *J. Biol. Chem.* **282**, 7982-7990.

Bourougaa, K., Naski, N., Boularan, C., Mlynarczyk, C., Candeias, M. M., Marullo, S. and Fåhraeus, R. (2010). Endoplasmic reticulum stress induces G2 cell-cycle arrest via mRNA translation of the p53 isoform p53/47. *Mol. Cell* **38**, 78-88.

Chen, L., Zhang, G. X., Zhou, Y., Zhang, C. X., Xie, Y. Y., Xiang, C., He, X. Y., Zhang, Q. and Liu, G. (2015). BAC transgenic mice provide evidence that p53 expression is highly regulated in vivo. *Cell Death Dis.* **6**, e1878.

Choi, M., Lee, H. and Rho, H. M. (2002). E2F1 activates the human p53 promoter and overcomes the repressive effect of hepatitis B viral X protein (Hbx) on the p53 promoter. *IUBMB Life* **53**, 309-317.

Di, R., Wu, X., Chang, Z., Zhao, X., Feng, Q., Lu, S., Luan, Q., Hemmings, B. A., Li, X. and Yang, Z. (2012). S6K inhibition renders cardiac protection against myocardial infarction through PDK1 phosphorylation of Akt. *Biochem. J.* **441**, 199-207.

Dony, C., Kessel, M. and Gruss, P. (1985). Post-transcriptional control of myc and p53 expression during differentiation of the embryonal carcinoma cell line F9. *Nature* **317**, 636-639.

Harris, S. L., Gil, G., Hu, W., Robins, H., Bond, E., Hirshfield, K., Feng, Z., Yu, X., Teresky, A. K., Bond, G. et al. (2005). Single-nucleotide polymorphisms in the p53 pathway. *Cold Spring Harb. Symp. Quant. Biol.* **70**, 111-119.

Haupt, Y., Maya, R., Kazaz, A. and Oren, M. (1997). Mdm2 promotes the rapid degradation of p53. *Nature* **387**, 296-299.

Jopling, C., Sleep, E., Raya, M., Marti, M., Raya, A. and Izpisua Belmonte, J. C. (2010). Zebrafish heart regeneration occurs by cardiomyocyte dedifferentiation and proliferation. *Nature* **464**, 606-609.

Kikuchi, K., Holdway, J. E., Werdich, A. A., Anderson, R. M., Fang, Y., Egnaczyk, G. F., Evans, T., MacRae, C. A., Stainier, D. Y. R. and Poss, K. D. (2010). Primary contribution to zebrafish heart regeneration by gata4(+) cardiomyocytes. *Nature* **464**, 601-605.

Kimura, W., Xiao, F., Canseco, D. C., Muralidhar, S., Thet, S. W., Zhang, H. M., Abderrahman, Y., Chen, R., Garcia, J. A., Shelton, J. M. et al. (2015). Hypoxia fate mapping identifies cycling cardiomyocytes in the adult heart. *Nature* **523**, 226-230.

Development (2017) 144, 580-589 doi:10.1242/dev.147827

Kubbutat, M. H. G., Jones, S. N. and Vousden, K. H. (1997). Regulation of p53 stability by Mdm2. *Nature* **387**, 299-303.

Laflamme, M. A. and Murry, C. E. (2005). Regenerating the heart. *Nat. Biotechnol.* **23**, 845-856.

Loffredo, F. S., Steinhauser, M. L., Gannon, J. and Lee, R. T. (2011). Bone marrow-derived cell therapy stimulates endogenous cardiomyocyte progenitors and promotes cardiac repair. *Cell Stem Cell* **8**, 389-398.

Mahmoud, A. I., Porrello, E. R., Kimura, W., Olson, E. N. and Sadek, H. A. (2014). Surgical models for cardiac regeneration in neonatal mice. *Nat. Protoc.* **9**, 305-311.

Masuda, S., Montserrat, N., Okamura, D., Suzuki, K. and Izpisua Belmonte, J. C. (2012). Cardiosphere-derived cells for heart regeneration. *Lancet* **379**, 2425-2426; author reply 2426-2427.

Naqvi, N., Li, M., Calvert, J. W., Tejada, T., Lambert, J. P., Wu, J., Kesteven, S. H., Holman, S. R., Matsuda, T., Lovelock, J. D. et al. (2014). A proliferative burst during preadolescence establishes the final cardiomyocyte number. *Cell* **157**, 795-807.

Porrello, E. R., Mahmoud, A. I., Simpson, E., Hill, J. A., Richardson, J. A., Olson, E. N. and Sadek, H. A. (2011). Transient regenerative potential of the neonatal mouse heart. *Science* **331**, 1078-1080.

Reich, N. C. and Levine, A. J. (1984). Growth regulation of a cellular tumour antigen, p53, in nontransformed cells. *Nature* **308**, 199-201.

Reisman, D., Elkind, N. B., Roy, B., Beamon, J. and Rotter, V. (1993). c-Myc trans-activates the p53 promoter through a required downstream CACGTG motif. *Cell Growth Differ.* **4**, 57-65.

Senyo, S. E., Steinhauser, M. L., Pizzimenti, C. L., Yang, V. K., Cai, L., Wang, M., Wu, T.-D., Guerquin-Kern, J.-L., Lechene, C. P. and Lee, R. T. (2013). Mammalian heart renewal by pre-existing cardiomyocytes. *Nature* **493**, 433-436.

Soonpaa, M. H., Zebrowski, D. C., Platt, C., Rosenzweig, A., Engel, F. B. and Field, L. J. (2015). Cardiomyocyte cell-cycle activity during preadolescence. *Cell* **163**, 781-782.

Vousden, K. H. and Lane, D. P. (2007). p53 in health and disease. *Nat. Rev. Mol. Cell Biol.* **8**, 275-283.